


Modeling multi-spectral paired-agent imaging (mPAI) to quantify available immune checkpoint proteins

A Thesis Submitted to the Faculty
In Partial Fulfillment of the Requirements for the Degree of
Bachelor of Arts
in
Engineering Sciences

by Abdibaset Ahmed Bare

Thayer School of Engineering
Dartmouth College
Hanover, New Hampshire

June 2025

Advisor: _____

Dr. Kimberley Samkoe

Associate Professor

Author: _____

Abdibaset Bare

Acknowledgements

I would like to express my sincere gratitude to Dr. Kimberley Samkoe and Dr. Divya Ravi for their invaluable mentorship and steadfast support, which have been instrumental since my freshman summer. As my academic advisor and research mentor, Dr. Samkoe—an Associate Professor at Dartmouth College and the Principal Investigator of the Samkoe Laboratory—introduced me to research and provided the foundational opportunity to join her lab. I am also deeply indebted to Dr. Divya Ravi, a recent graduate of the Molecular and Cellular Biology program at the Guarini School of Graduate and Advanced Studies, whose exceptional patience and dedication in training me - while simultaneously completing her dissertation - greatly contributed to my development as a research assistant. I also extend my thanks to the entire Samkoe Laboratory, especially Sassan Hodge, Veronica Torres, and Sanjana Pannem, for their collaborative spirit and consistent support in experimental design and data analysis.

This work was generously supported in part by summer internship funding from the E.E. Just Program and by a research funding award from the Dartmouth Cancer Center's Student Cancer Research in Immunology Projects (SCRIP), supported under grant number 5P30CA023108-45.

Abstract

Immune checkpoint inhibitors (ICIs) targeting the programmed cell death protein 1 (PD1) and its ligand, programmed death-ligand 1 (PDL1), have transformed cancer immunotherapy by disrupting inhibitory signaling pathways. However, only a subset of patients achieve durable responses. This limitation is in part due to current diagnostic approaches that rely on static immunohistochemical (IHC) assessments of PDL1 expression, which fail to capture its dynamic and functional availability. In addition, PDL1 can become unavailable for PD1 binding through *cis*-interactions with CD80, further complicating its reliability as a predictive biomarker.

To address these challenges, this work develops and validates a paired-agent imaging (PAI) approach using fluorescence-based imaging to dynamically quantify both the expression and functional availability of PDL1 *in vitro*. A multi-spectral PAI (mPAI) method was first implemented to measure the total expression of the PD1, PDL1, and CD80 receptors using four spectrally distinct antibody–fluorophore conjugates. Diffusion coefficients and corresponding times were experimentally determined in cell-free tissue-mimicking phantoms and used to establish incubation times for imaging in tissue mimicking phantoms containing tumor cells.

A second project focused on quantifying the fraction of PDL1 available for PD1 binding using soluble PD1 protein. The binding potential was measured under both unstimulated and interferon-gamma (IFN- γ)–stimulated conditions in lymphoma cells. Results demonstrated that IFN- γ stimulation increased both PDL1 expression thus the binding potential, indicating increased receptor availability. Collectively, these methods enable the distinction between total PDL1 expression and its functional accessibility for PD1 engagement, providing a refined framework for evaluating ICI response and advancing the development of imaging-based biomarkers.

Contents

1	Introduction	2
1.1	Background and Motivation	2
1.2	Paired Agent Imaging	3
1.3	Thesis Structure	4
2	Antibody and soluble protein diffusion coefficients	6
2.1	Introduction	6
2.2	Methods	9
2.3	Results	9
2.4	Discussion	11
3	Selection of fluorophore combinations using liquid phantoms	13
3.1	Introduction	13
3.2	Methods	14
3.2.1	Liquid phantom protocol for linearity test	14
3.2.2	Liquid phantom protocol for combination experiments	15
3.3	Results	16
3.4	Discussion	20
4	Paired Agent Imaging with Soluble PD1	21
4.1	Introduction	21
4.2	Methods	22
4.3	Results	23
4.4	Discussion	25
5	Future work and global conclusions	27
5.1	Conclusions	27
5.2	Future work for mPAI	27
5.3	Future work for PAI with soluble PD1	28

List of Tables

2.1	Summary of mean diffusion coefficients and diffusion times	10
-----	--	----

List of Figures

1	FWHM technique	7
2	Representative diffusion analysis	8
3	Comparison of diffusion coefficients	11
4	Combination experiments set up	16
5	Linearity test results	17
6	Combination experiments results in 700nm channel	18
7	Combination experiments results in 800nm channel	19
8	Binding Potential-Total receptor comparison	24
9	Binding potential fits	25

Chapter 1: Introduction

1.1 Background and Motivation

Programmed cell death protein 1 (PD1) is an immune checkpoint receptor expressed on activated T cells. It functions as an inhibitory receptor, helping to limit excessive immune responses and maintain immune tolerance. PD1 binds to its ligand, programmed death-ligand 1 (PDL1), which is expressed in antigen-presenting cells (APCs) and many other cell types, including normal and tumor cells. This interaction sends an inhibitory signal to the T cell, reducing its activity and preventing potential collateral tissue damage or autoimmunity. Tumor cells can exploit this mechanism by expressing PDL1, falsely signaling to activated T cells that they are normal cells. This evasion not only facilitates tumor survival but also contributes to T-cell exhaustion and dysfunction [1, 2, 3, 4].

Immune checkpoint inhibitors (ICI), such as anti-PD1 and anti-PDL1 monoclonal antibodies, pharmacologically block the PD1:PDL1 interaction. Despite their success in improving overall survival in several difficult-to-treat cancers, only a minority of patients experience durable clinical benefits [5, 6]. Clinically, anti-PD1 therapy is often recommended based on tumor PDL1 expression levels [7]. Currently, immunohistochemical staining (IHC) of primary tumors is the standard diagnostic method for assessing PDL1 expression. However, IHC provides only a static snapshot and does not capture the dynamic nature of PDL1 availability. PDL1 expression is conditional, often transient, and is induced by local immune activity, particularly T cell infiltration.

As a result, IHC can misclassify tumors as negative for PDL1 if inflammation is absent at the time of biopsy [8].

Recently, it has been shown that PDL1 can also *cis*-dimerize with CD80 on the same cell surface. This *cis*-interaction reduces the amount of PDL1 available for PD1 binding, potentially impairing the efficacy of therapies targeting this pathway [9, 3, 10]. As a result, surface PDL1 levels alone may not reflect the functional availability of PDL1, complicating its use as a predictive biomarker for the ICI response.

Given the limitations of static diagnostic methods like immunohistochemistry, there is a critical need to develop a dynamic approach to assess the engagement of PDL1 with both PD1 and CD80. Paired agent imaging (PAI) has previously been demonstrated as a quantitative fluorescence imaging technique to measure receptor availability *in vivo* [11]. Building on this approach, the goal of this research is to develop an *in vivo* optical fluorescence imaging technique capable of simultaneously quantifying the expression of PD1, PDL1, and CD80, as well as determining the fraction of PDL1 available for PD1 binding. The methodology is described in detail below.

1.2 Paired Agent Imaging

PAI is a fluorescence-based molecular imaging technique that involves the simultaneous administration of a receptor-targeted imaging agent and an untargeted control agent, each conjugated to spectrally distinct fluorescent dyes but exhibiting matched pharmacokinetic profiles. By enabling the separation of specific binding from non-specific uptake, PAI’s computation model facilitates the quantitative estimation of *in vivo* receptor concentration and availability.

To evaluate immune checkpoint receptor expression, we developed a multi-spectral paired-agent imaging (mPAI) approach capable of simultaneously quantifying the concentrations of PD1, PDL1, and CD80. This methodology involved the co-administration of four monoclonal antibodies: three receptor-targeted antibodies—anti-PD1, anti-PDL1, and anti-CD80 and one untargeted isotype control (IgG). Each antibody was conjugated to a unique fluorophore, enabling multiplexed, spectrally resolved quantification of receptor expression.

Following the quantification of PDL1 expression, a two-agent PAI experiment was conducted to assess receptor availability. This experiment employed a fluorescently labeled soluble PD1 protein as the targeted agent and a spectrally distinct free dye as the untargeted control. Receptor availability was quantified via calculation of the binding potential, reflecting the accessible fraction of PDL1 capable of engaging PD1.

The PAI experiments utilized near-infrared fluorescent dyes: IRDye680LT (IR680), Alexa Fluor 700 (AF700), Alexa Fluor 750 (AF750), and IRDye800CW (IR800). Imaging was performed using the Pearl® Imaging System, which incorporates two optical detection channels centered at 700 nm and 800 nm. IR680 and AF700 were detected in the 700 nm channel, while AF750 and IR800 were detected in the 800 nm channel, ensuring minimal spectral overlap, and enabling accurate fluorophore discrimination.

1.3 Thesis Structure

This thesis is divided into two main projects. The first is part of a larger project aimed at developing an mPAI framework for simultaneously quantifying multiple immune checkpoint receptors, including PD1, PDL1, and CD80. My contribution focuses specifically on diffusion experiments to determine the diffusion coefficients and times. These diffusion times are critical for establishing appropriate incubation durations in tissue mimicking phantoms inoculated with tumor cells, ensuring reliable agent distribution prior to imaging. A comprehensive account of these diffusion studies, along with the associated experimental protocols, is presented in Chapter 2.

The second project involves a PAI approach using soluble PD1 to quantify the fraction of PDL1 receptors that are functionally available for PD1 binding. A detailed account of this work is provided in Chapter 4. The general structure of the thesis is as follows:

- Chapter 2: Antibody and soluble protein diffusion coefficients - Description of tissue mimicking phantom use for determining diffusion parameters.

- Chapter 3: Selection of fluorophore combinations using liquid phantoms - Identification of spectrally compatible dyes and assessment of signal interference.
- Chapter 4: PAI: Quantification of functionally available PDL1 for PD1 binding.
- Chapter 5: Future work and global conclusions.

Chapter 2: Antibody and soluble protein diffusion coefficients

2.1 Introduction

To validate the feasibility of both mPAI for quantifying the expression of multiple immune checkpoint receptors and PAI with soluble PD1 to measure receptor availability, we first conducted diffusion experiments in tissue mimicking phantoms without cells. These experiments were designed to determine the diffusion coefficients and corresponding diffusion times of fluorescently labeled imaging agents. The results informed the appropriate incubation times needed before imaging experiments in tissue mimicking phantoms with tumor cells.

In biological systems, molecular diffusion arises from the random thermal motion of particles and is a fundamental mechanism that governs the transport of substances within tissues. This process is particularly critical in the context of molecular imaging, where the spatial and temporal distribution of imaging agents determines the accuracy of quantitative assessments.

To characterize diffusion behavior *in vitro*, we used the cell-free, agarose-based tissue mimicking phantoms whose protocol is outlined in Section 2.2. Fluorescent images were acquired using the Pearl imaging system, and the images were analyzed using MATLAB. A region of interest (ROI) was defined around the central hole where the fluorescent agent was introduced, using an ROI generator implemented in MATLAB. To account for variability in the shape of the holes in the

agar, the ROI was rotated at four angles: 0° , 45° , 90° , and 135° . Pixel intensities within the ROI were summed column-wise to generate one-dimensional intensity profiles for each orientation.

To quantify radial diffusion from the hole containing the dye at the center of the well, the full-width at half-maximum (FWHM) method was applied after subtracting the background signal acquired before dye addition. The diffusion distance at time, t , was therefore determined based on the width of the profile at half its maximum intensity, as illustrated in Figure 1.

To determine the diffusion coefficient, we modeled the spread of dye within the agarose phantom as a two-dimensional random walk originating from the hole that contains the dye. The diffusion behavior was quantified using the mean squared displacement (MSD) relation shown in Equation 2.1:

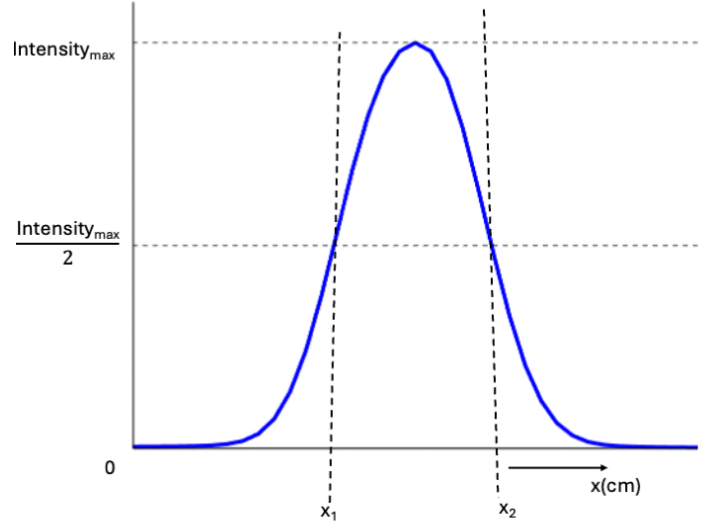


Figure 1. FWHM technique illustration. The curve shows fluorescence intensity as a function of x (cm). FWHM is the width at half-maximum between x_1 and x_2 .

$$\langle r^2 \rangle = 4Dt \quad (2.1)$$

where D is the diffusion coefficient (cm^2/s) and t is the time of image acquisition(s).

The experimental time (t_{exp}) required for the fluorescent antibody to distribute evenly throughout the tissue mimicking phantom was determined using Equation 2.1, but using the depth of the tissue mimicking phantom ($x = 0.106\text{cm}$) and the experimentally determined

diffusion coefficient (D) above:

$$t_{exp} = \frac{x^2}{4D} = \frac{(0.106cm)^2}{4D} \quad (2.2)$$

Figure 2 presents representative ROI images rotated at four angles (0° , 45° , 90° , and 135°), together with the corresponding intensity peak profiles and $\langle r^2 \rangle$ versus *time* plots used to calculate the diffusion coefficients.

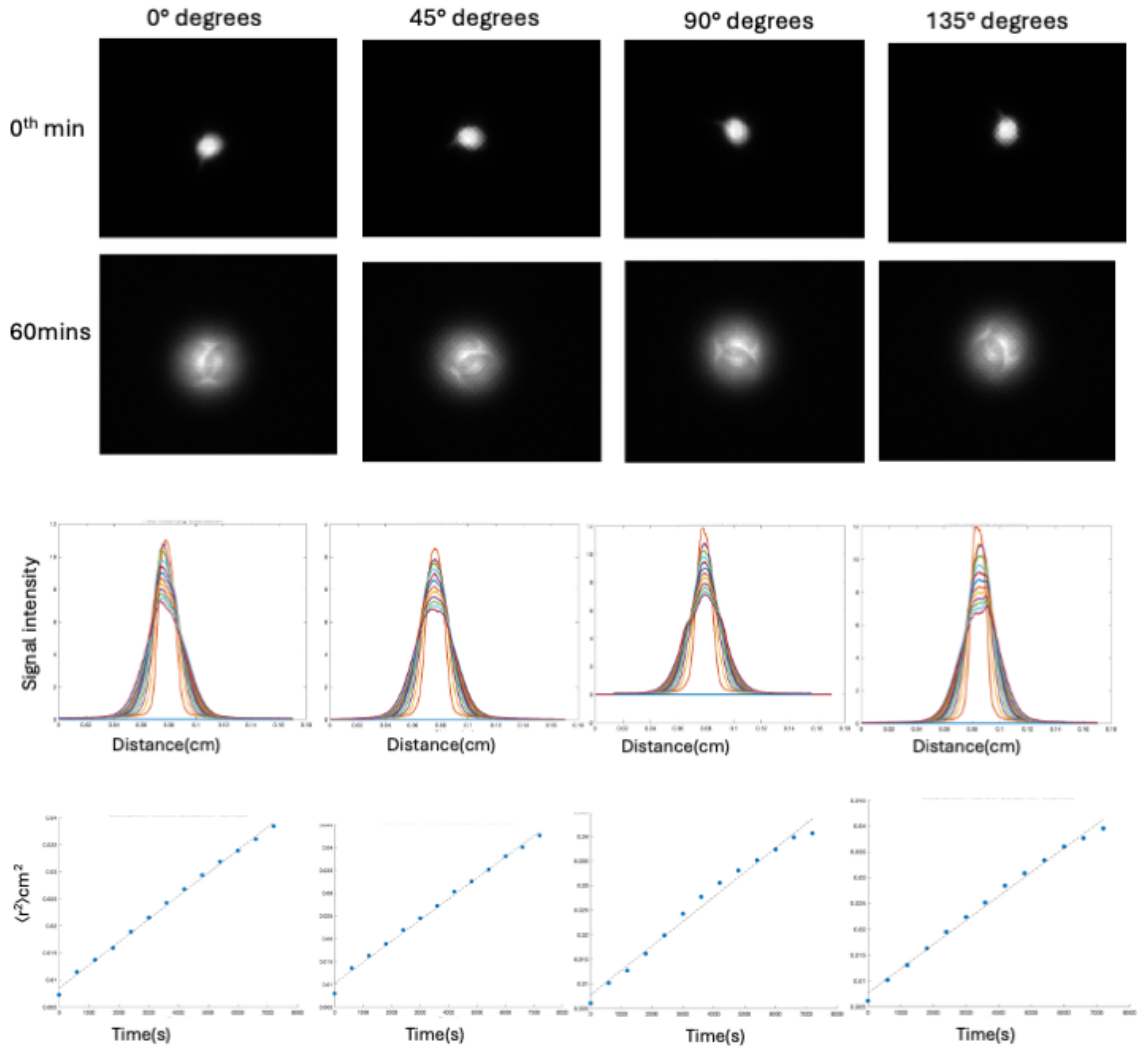


Figure 2. Representative diffusion analysis across four angular directions (0° , 45° , 90° , and 135°). Top panels show fluorescence images of the ROI at 0 and 60 minutes. Middle panels display signal intensity profiles as a function of distance from the center, extracted from each time point and angle. Bottom panels present mean squared displacement, $\langle r^2 \rangle$, versus time plots corresponding to each orientation, used to calculate diffusion coefficients.

For the mPAI experiments, three monoclonal antibodies were used as targeted imaging agents: anti-PD1 was conjugated to IR680, anti-PDL1 to AF750, and anti-CD80 to AF700. An untargeted antibody (IgG) was labeled with IR800. For the PAI experiment involving soluble proteins, a soluble PD1 protein was labeled with IR800 and paired with free IR680 as an untargeted control. These fluorophore-protein pairings were selected based on preliminary liquid phantom experiments (described in Chapter 3) that evaluated fluorescence intensity, linearity, and spectral interference across the detection channels of the Pearl imaging system.

2.2 Methods

Agarose-based tissue mimicking phantoms protocol

To prepare the tissue phantom, 0.3 g of agarose powder was mixed with 50 mL of phosphate buffered saline (PBS) and heated on a hot plate while stirring until the agarose was fully dissolved, yielding a 0.6%(w/v) agarose solution. The solution was then cooled to approximately 39°C before combining 10 mL of the agarose solution with 10 mL of warm PBS to create a mixture of agarose 0.3%(w/v). A volume of 5000 μ L of the 0.3%(w/v) agarose mixture was added to each well of a dark-colored, four-well 3D-printed plate, with each well having a diameter of 35.34 mm and a depth of 19.10 mm. The plate was placed in a digital dry bath and incubated for 15 – 30 minutes to allow the agarose to solidify. After gelation, a central hole was made in the agarose of each well using a 16-gauge $\times \frac{1}{2}$ " Luer stub needle. A background fluorescence image was acquired prior to dye introduction. Then, 12 μ L of fluorescent dye was placed in the hole. After dye introduction, fluorescence images were acquired at 5-minute intervals over a 60-minute period. Background images were used for noise subtraction during image analysis.

2.3 Results

As shown in Figure 3a, diffusion analysis demonstrated that Alexa Fluor conjugated antibodies exhibited significantly higher diffusion coefficients and shorter diffusion times compared to IRDye

conjugated antibodies. Specifically, anti-CD80 labeled with AF700 and anti-PDL1 labeled with AF750 had diffusion coefficients of $(9.00 \pm 0.27) \times 10^{-7} \text{ cm}^2/\text{s}$ and $(8.35 \pm 0.26) \times 10^{-7} \text{ cm}^2/\text{s}$, respectively. In contrast, anti-PD1 labeled with IR680 and the untargeted IgG control labeled with IR800 had lower diffusion coefficients of $(5.47 \pm 0.48) \times 10^{-7} \text{ cm}^2/\text{s}$ and $(4.93 \pm 0.77) \times 10^{-7} \text{ cm}^2/\text{s}$, respectively. As a result, Alexa Fluor conjugated agents diffused through the 10.6 mm agarose phantom more rapidly, reaching near-equilibrium conditions within 55.3 ± 0.14 minutes for anti-CD80 and 56.6 ± 1.8 minutes for anti-PDL1. In contrast, the IReDye-labeled agents had longer diffusion times, with anti-PD1 reaching equilibrium at 86.20 ± 7.8 minutes and IgG control at 99.7 ± 14 minutes. Based on these results, a standardized incubation period of 120 minutes was adopted for all subsequent mPAI imaging experiments of tissue-mimicking phantoms with cells.

As shown in Figure 3b, the difference between the diffusion coefficients of the free dye IR680, $(4.93 \pm 0.0017) \times 10^{-6} \text{ cm}^2/\text{s}$, and the soluble PD1 conjugated to IR800, $(1.16 \pm 0.0027) \times 10^{-6} \text{ cm}^2/\text{s}$, is not statistically significant. Their diffusion times were 34.2 ± 4.0 minutes and 42.2 ± 9.8 minutes, respectively. Based on these results, a 60-minute incubation period was established for the PAI experiments using soluble PD1. A summary of these data is provided in Table 2.1.

Table 2.1: Summary of mean diffusion coefficients and diffusion times

Imaging Agent	Mean (standard deviation)	
	Diffusion Coefficient (cm^2/s)	Time (mins)
anti-PDL1-AF750	$(8.35 \pm 0.26) \times 10^{-7}$	56.6 ± 1.8
anti-PD10IR680	$(5.47 \pm 0.48) \times 10^{-7}$	86.2 ± 7.8
anti-CD80-AF700	$(9.00 \pm 0.27) \times 10^{-7}$	55.3 ± 1.4
anti-IgG-IR800	$(4.93 \pm 0.77) \times 10^{-7}$	99.7 ± 14.0
IR800 (free dye)	$(4.93 \pm 0.017) \times 10^{-6}$	34.2 ± 4.0
Soluble PD1-IR800	$(1.16 \pm 0.027) \times 10^{-6}$	42.2 ± 9.8

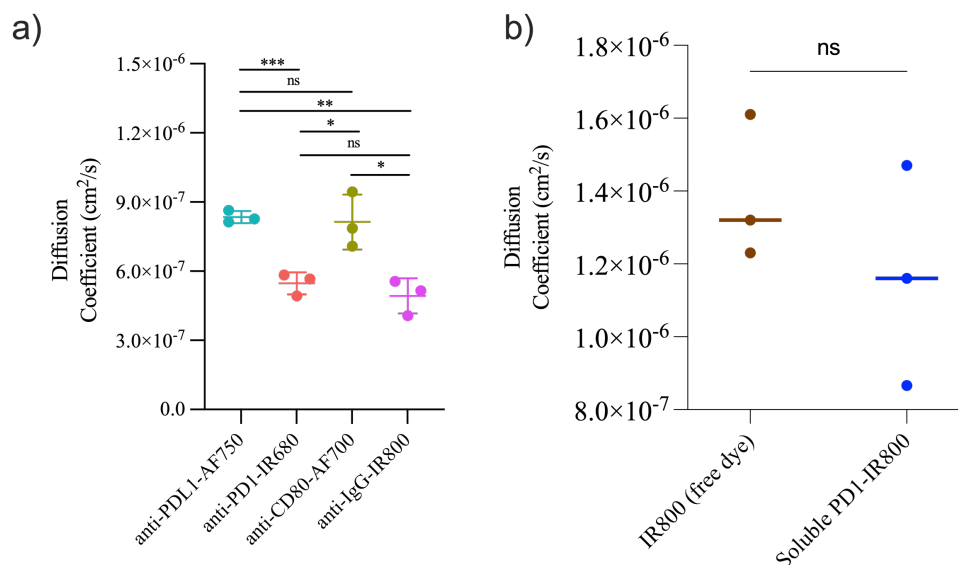


Figure 3. Comparison of the Diffusion Coefficients of Different Imaging Agents. (a) Distribution of diffusion coefficients for antibodies conjugated to fluorophores. Alexa Fluor-conjugated antibodies (PDL1-AF750 and CD80-AF700) exhibited significantly higher diffusion coefficients compared to IRDye-conjugated antibodies (PD1-IR680 and IgG-IR800). (b) Distribution of diffusion coefficients for free IR800 dye and soluble PD1-IR800. Asterisks indicate statistically significant differences, while “ns” denotes non-significant differences.

2.4 Discussion

This study demonstrates the feasibility of using mPAI and PAI with soluble PD1 in tissue mimicking phantoms to quantify the expression and availability of the immune checkpoint receptor, respectively. By modeling diffusion as a two-dimensional random walk and applying the mean squared displacement (MSD) relation, we were able to experimentally determine the diffusion coefficients of various fluorescently labeled antibodies and proteins and calculate the corresponding incubation times required for the imaging to diffuse through the 10.6mm agar layer before imaging experiments of tissue mimicking phantoms with tumor cells.

Our findings show that antibodies labeled with AF750 and AF700 exhibited significantly higher diffusion coefficients than those labeled with IR680 and IR800. This difference suggests the physicochemical properties of the fluorophores, particularly molecular weight because smaller

molecules diffuse more rapidly and hydrophilicity substantially influences diffusion behavior in the agarose environment. These variations directly affect experimental timing, as faster diffusion results in shorter times to reach equilibrium.

For mPAI, the calculated diffusion times for the various agents ranged from approximately 55 to 100 minutes. For PAI with soluble PD1, these times were shorter, ranging from 34 to 42 minutes. This difference is attributed to the larger molecular weights of the antibodies used in mPAI compared to the proteins and free dyes used in PAI with soluble PD1. To ensure sufficient binding and to account for slight variations between agents, we standardized the incubation period: 120 minutes for mPAI and 60 minutes for PAI with soluble PD1. This buffered approach ensures that all agents have ample time to reach binding equilibrium before imaging, minimizing the risk of dye wash-off before all imaging agents fully diffuse through the 10.6-mm agar layer.

These findings laid the groundwork for utilizing tissue mimicking phantom with tumor cells to evaluate the binding potential of various imaging agents. Importantly, the ability to capture real-time differences in diffusion and binding supports the broader aim of developing a dynamic platform to quantify PDL1 expression and availability using mPAI and PAI with soluble PD1. This approach advances the potential for imaging-based biomarkers to improve the prediction of positive response to immune checkpoint inhibitor (ICI) treatments.

Chapter 3: Selection of fluorophore combinations using liquid phantoms

3.1 Introduction

For the PAI experiment utilizing soluble PD1, it was necessary to identify two fluorescent dyes with spectrally distinct emission profiles suitable for concurrent detection. To guide the selection of appropriate dye pairs, we conducted a series of liquid phantom experiments designed to assess both the linearity of the fluorescence signal and the degree of spectral interference between fluorophores.

Liquid phantoms are optically tunable models designed to mimic the absorption and scattering properties of biological media. In this study, liquid phantoms were employed to evaluate the spectral compatibility of our four fluorescent dyes, ensuring the selection of two dyes with minimal signal overlap and enabling accurate quantification of individual receptor concentrations. To validate dye selection, we first conducted linearity tests for each dye individually, followed by combination experiments to assess potential spectral interference. These procedures will be discussed in detail in Section 3.2.

Linearity tests were performed to determine whether the intensity of the fluorescence signal increased proportionally with the concentration of the dye. This allowed us to identify the linear response range for each fluorophore. Based on the results of the linearity test, we selected a single reference signal intensity that fell within the linear range for all dyes. This signal value was then used to determine the corresponding concentration of each dye in the combination experiments.

3.2 Methods

3.2.1 Liquid phantom protocol for linearity test

To evaluate the linearity of fluorescence signal intensity with respect to dye concentration, we conducted liquid phantom experiments for each fluorescent dye. The dyes were imaged in the detection channels corresponding to their peak excitation wavelengths: IR680 and AF700 in the 700 nm channel and AF750 and IR800 in the 800 nm channel. IR680 and AF700 were prepared and imaged in a single 96 well plate, as were AF750 and IR800. For each dye, a series of eight concentrations was prepared, $0.1nM$, $1nM$, $10nM$, $20nM$, $40nM$, $60nM$, $80nM$, and $100nM$. Each concentration was tested in triplicate, resulting in 24 wells per dye to ensure statistical robustness.

Each well contained a total volume of 300 μL , composed of 15 μL of 20% Intralipid, 15 μL of 20% bovine serum albumin (BSA), a calculated volume of dye stock solution, and PBS to complete the volume. The volume of dye stock required to achieve the final target concentration (C_{final}) was determined using the dilution equation 3.1:

$$V_{dye} = \frac{C_{final} \cdot V_{final}}{C_{dye}} \quad (3.1)$$

where V_{dye} is the volume of dye stock solution, C_{final} is the desired final concentration, V_{final} is the total volume of the well, and C_{dye} is the concentration of the dye stock solution. The volume of PBS was adjusted accordingly:

$$V_{PBS} = V_{final} - V_{dye} - V_{Intralipid} - V_{BSA} \quad (3.2)$$

Three replicate wells containing no dye were included on each plate for background subtraction. The image was taken in the Pearl imaging system, and the resulting fluorescence image was analyzed with ImageJ.

3.2.2 Liquid phantom protocol for combination experiments

Following the determination of the linear response range and the selection of a uniform fluorescence intensity value, we calculated the corresponding dye concentrations that produced this signal within a 300 μL volume. Each dye was then imaged individually and in binary combinations with dyes from the opposite detection channel, for example, IR680 alone and in combination with AF750 and IR800.

As in the linearity experiments, each well was prepared with a total volume of 300 μL , including 15 μL of 20% Intralipid, 15 μL of 20% BSA, the required volume (s) of the dye stock solution and the volume of PBS. Individual volumes of each dye were calculated using the same dilution equation 3.1 and PBS was added to complete the total volume. A schematic of the 96-well plate layout is provided in Figure 4.

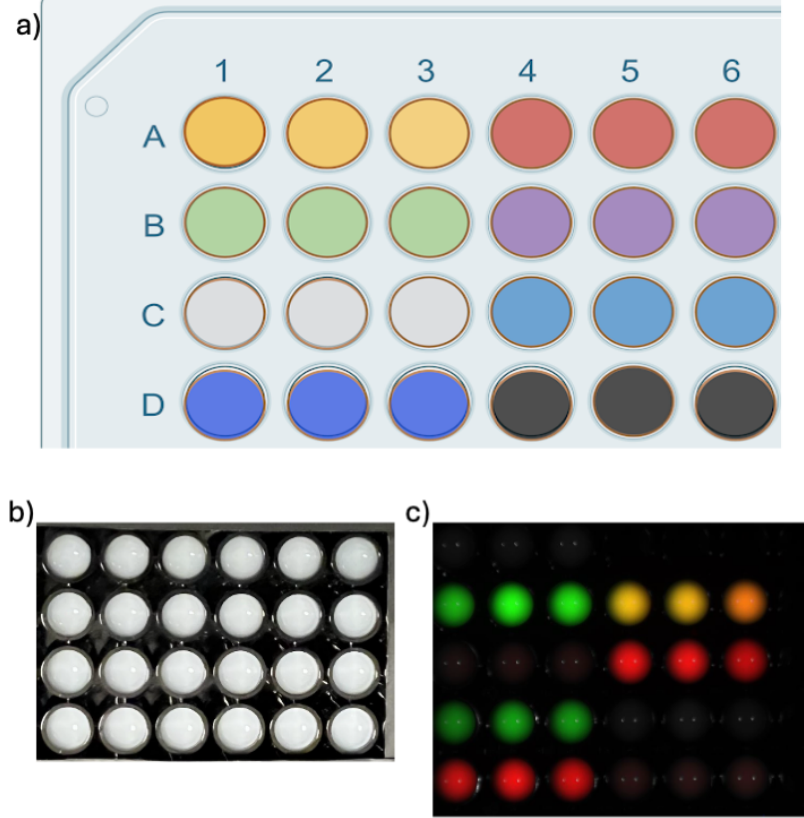


Figure 4. Combination fluorophore experiments set up. (a) Plate map showing the layout of dye combinations and controls in a 96-well plate. Wells A1-A3 contain combinations of AF700 with IR800; A4-A6 contain IR680 with IR800. Wells B1-B3 contain AF700 with AF750; B4-B6 contain IR680 with AF750. Row C contains single-agent controls: IR800 (C1-C3) and AF750 (C4-C6). Row D contains IR680 (D1-D3) and AF700 (D4-D6). Wells E1-E3 are dye-free controls. (b) Image of the 96-well plate before imaging. (c) Representative fluorescence image from the Pearl Imaging System showing spectral separation of the fluorophores.

3.3 Results

As shown in Figure 5, all four dyes exhibited a linear correlation between concentration and signal intensity. To allow a consistent comparison between the fluorescent dyes, a signal intensity value of 0.2 was used, within the linear range for all dyes, to determine the corresponding concentrations in the liquid combination phantom experiments. The concentration required to reach this signal varied by dye: AF700 required the lowest concentration ($21.30nM$), followed by AF750 ($46.28nM$), IR680 ($92.68nM$), and IR800 ($282.00nM$).

In the combination experiments, fluorescence intensity measurements were collected for individual dyes and their binary mixtures using ImageJ. These analyzed results are summarized in Figures 6 and 7.

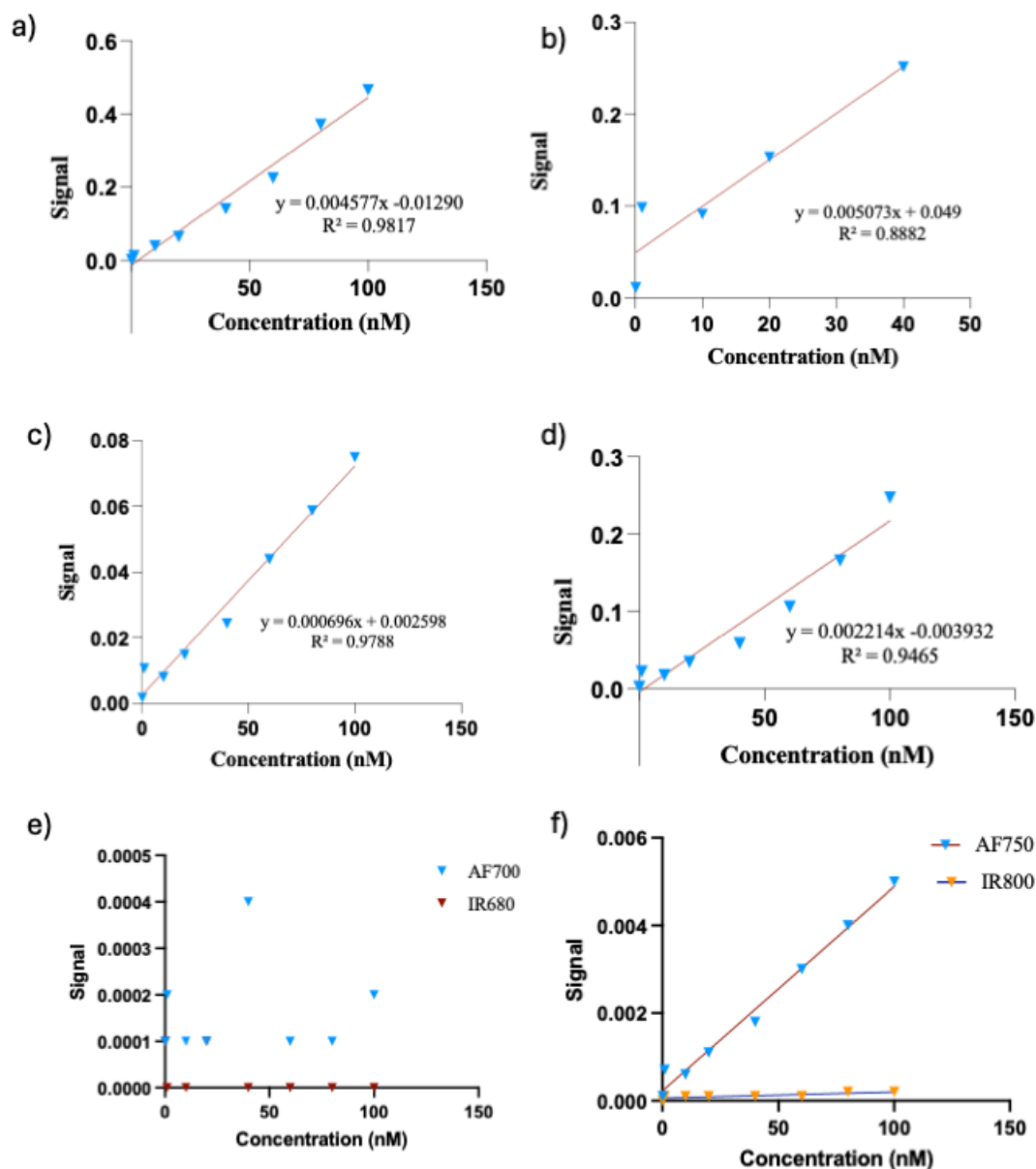


Figure 5. Linearity of signal intensity as a function of dye concentration in the 700 nm and 800 nm detection channels. (a-d) Calibration curves demonstrate linear relationships between dye concentration and signal intensity for each fluorophore in its primary detection channel: (a) IR680 and (b) AF700 in the 700 nm channel; (c) AF750 and (d) IR800 in the 800 nm channel. (e-f) Signal contribution from dyes in their non-primary detection channels (i.e., bleed-through): (e) IR680 and AF700 in the 800 nm channel; (f) AF750 and IR800 in the 700 nm channel.

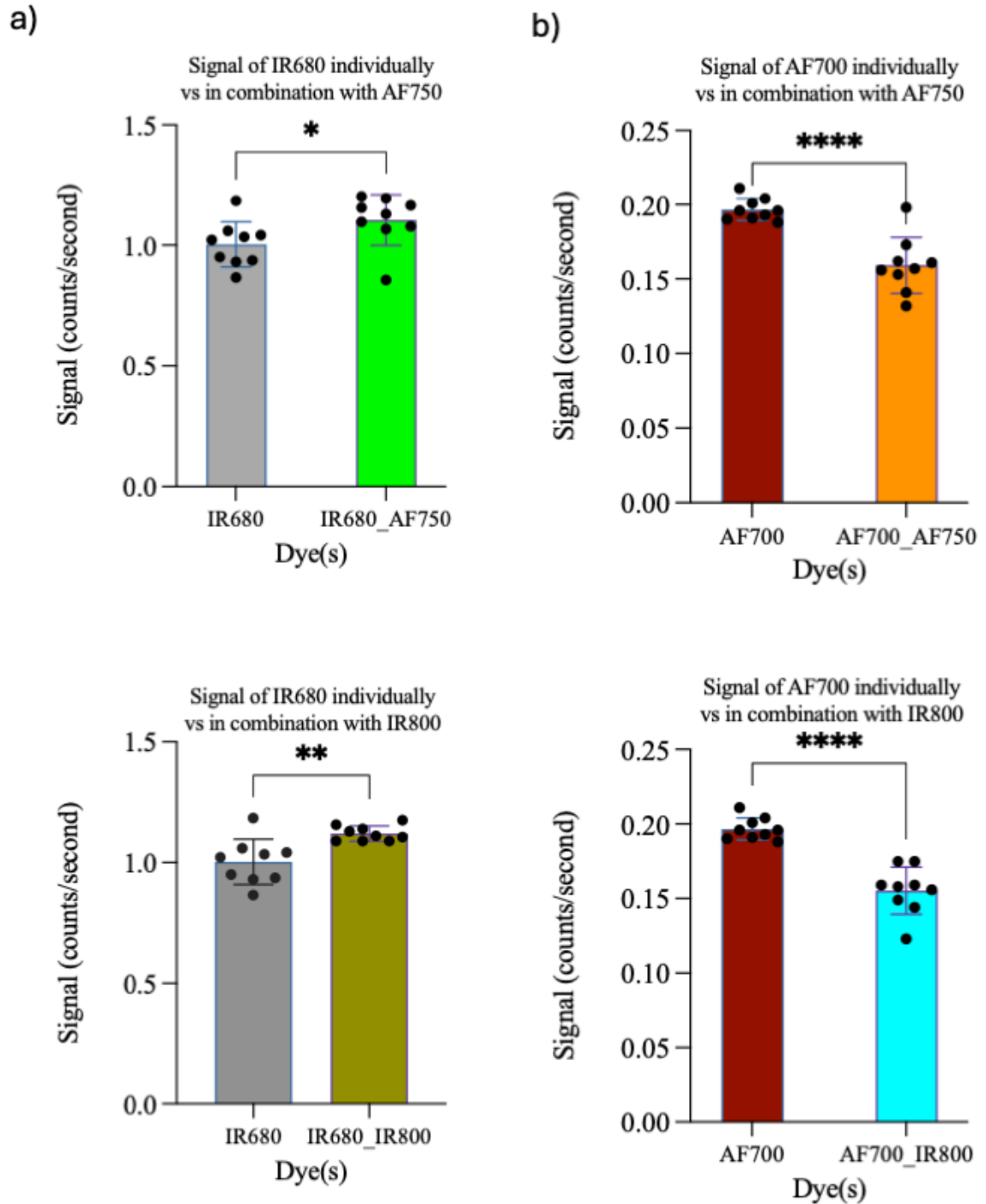


Figure 6. Fluorescence signal intensity comparisons in the 700 nm channel for individual dyes and binary combinations. (a) Signal intensity of IR680 alone vs. in combination with AF750 (top) and IR800 (bottom). (b) Signal intensity of AF700 alone vs. in combination with AF750 (top) and IR800 (bottom). Compared to AF700, IR680 showed minimal signal change when combined with AF750 or IR800, indicating lower spectral cross-talk.

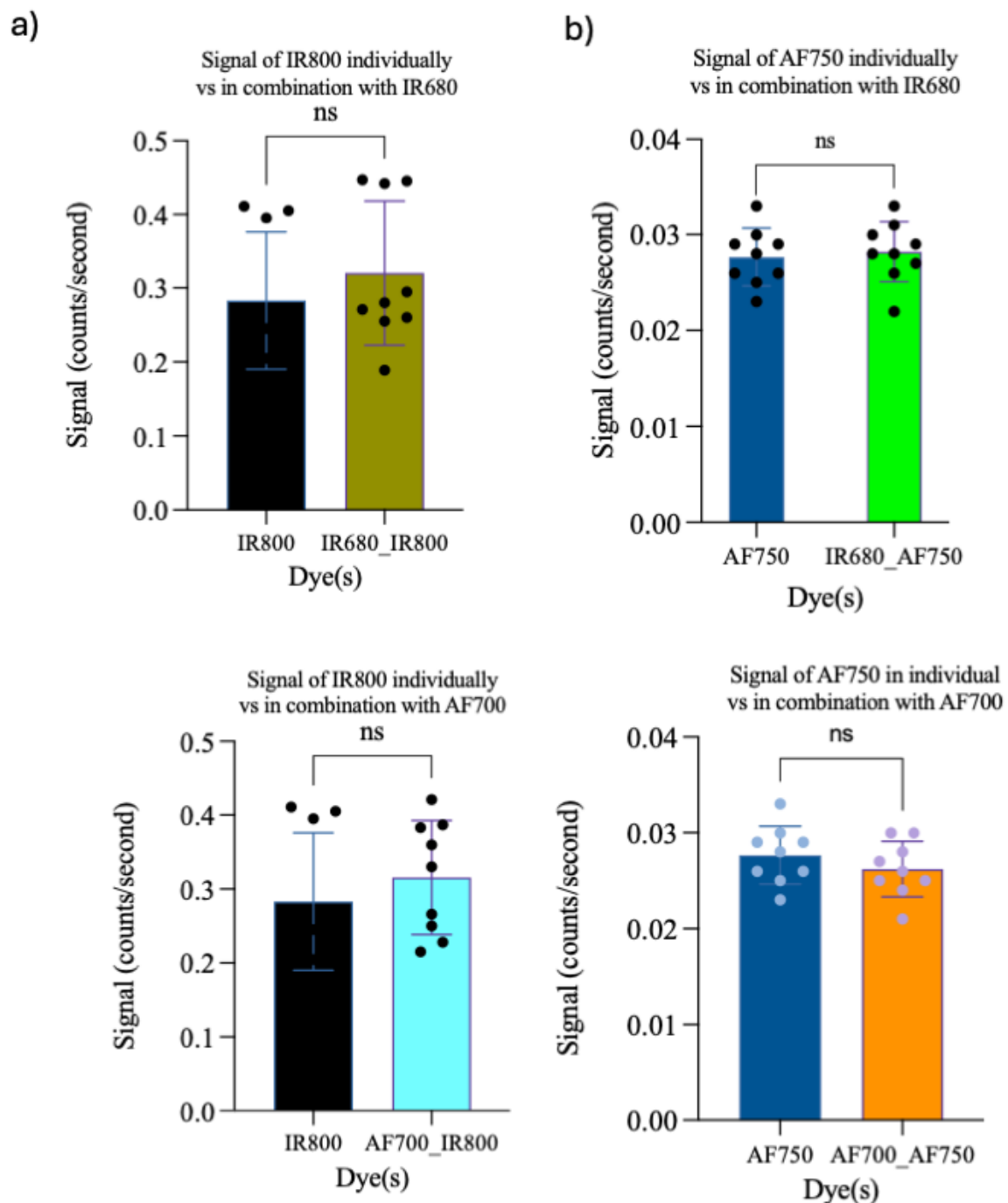


Figure 7. Fluorescence signal intensity comparisons in the 800 nm channel for individual dyes and binary combinations. (a) Signal intensity of AF750 alone vs. in combination with IR680 (top) and AF700 (bottom). (b) Signal intensity of IR800 alone vs. in combination with IR680 (top) and AF700 (bottom). No significant changes in signal were observed, indicating minimal spectral interference in the 800 nm channel.

3.4 Discussion

The liquid phantom experiments enabled quantitative assessment of fluorescence linearity and spectral compatibility across four candidate dyes for use in PAI. As shown in Figure 5, each dye demonstrated a linear relationship between signal intensity and concentration in the experimental range. These linearity data were subsequently employed to determine appropriate dye concentrations for multi-dye combination experiments.

In the combination experiments, analysis of the 700 nm channel revealed significant differences in signal intensity between individual dyes AF700 and IR680 and their combinations with AF750 and IR800. However, the observed difference in signal for IR680 was less significant than for AF700, indicating reduced cross-talk when IR680 is combined with AF750 or IR800. Consequently, IR680 was selected for the 700 nm channel to serve as our untargeted agent.

For the 800 nm channel, no significant differences in signal intensity were observed between AF750 and IR800, and their combinations with IR680 and AF700. However, as illustrated in Figure 5f, the linearity tests showed that IR800 contributed less signal to the 700 nm channel compared to AF750, indicating reduced spectral bleed-through into the 700 nm channel. This reduced spectral interference led to the selection of IR800 for the 800 nm channel, designated for conjugation to soluble PD1. These results are summarized in Figures 6 and 7.

Chapter 4: Paired Agent Imaging with Soluble PD1

4.1 Introduction

After quantification of PDL1 expression in lymphoma tumor cells using mPAI, the next objective was to determine the fraction of PDL1 available for binding to PD1. PDL1 does not only interact in *trans* with PD1, it can also form *cis*-dimers with CD80 on the same cell surface [10]. This *cis*-interaction sequesters PDL1 and renders it functionally unavailable for PD1 binding. To quantify the available PDL1, that is, the fraction capable of binding PD1, we used a PAI approach. In this experiment, the targeted agent consisted of a fluorescently labeled soluble PD1 protein, while the untargeted agent was a spectrally distinct free dye.

As in the mPAI experiments, the accurate quantification depends on the careful selection of dyes with compatible optical and detection properties. To this end, preliminary liquid phantom experiments were conducted to identify two fluorophores suitable for simultaneous imaging. Linearity assessments were performed to determine the concentration ranges over which each dye exhibited a linear fluorescence response. Subsequently, dye combination experiments were conducted to evaluate the spectral crosstalk between the 700 nm and 800 nm imaging channels. The combination experiments enabled the selection of dye pairs that could be imaged concurrently without compromising signal specificity.

After the selection of suitable dye pairs, the next step involved determining the optimal incubation times for these selected pairs with their respective conjugated proteins. To achieve this, we conducted diffusion experiments utilizing tissue-mimicking phantoms without cells for both

the targeted and untargeted agents. This was followed by tissue-mimicking phantom experiments with lymphoma cells. To quantify the available PDL1 receptors for PD1 binding, a binding potential analysis was performed.

4.2 Methods

Agarose with cells tissue mimicking phantoms

To prepare tissue mimicking phantoms, 0.3 g of agarose powder was dissolved in 50 mL of PBS by heating the mixture on a hot plate with continuous stirring until agarose was fully solubilized, resulting in a 0.6%(w/v) agarose solution. The solution was then cooled to approximately 39°C before use. Three experimental conditions were prepared: a control condition in which 0.6%(w/v) agarose was combined with 500 µL of PBS without any cells; an unstimulated cell condition in which 500 µL agarose solution was mixed with 500 µL of PBS containing 25 million lymphoma cells; and a stimulated condition in which 25 million Lymphoma cells were pre-treated with interferon-gamma (IFN- γ) for 24 hours, suspended in 500 µL of PBS, and mixed with 500 µL of the agarose solution. Before the introduction of imaging agents, a background fluorescence image was acquired for each well. Then, 1000 µL of solution, comprising a mixture of the targeted agent, untargeted agent, and PBS, was added to each well and incubated for a predetermined incubation time of 60 minutes. Following incubation, an image was captured, after which the phantom was rinsed with PBS for 5 minutes. The supernatant was removed and another image was taken. This rinsing process was repeated 15 times to monitor the clearance and agent retention within the phantom over time.

To analyze the cells shown in Figures 8a and 8b, a circular ROI was drawn using MATLAB, and the resulting ROI was analyzed with the rinsing paired agent model (rpam) algorithm developed by Xu et al. [12]

To determine the expression levels of PDL1, PD1, and CD80 under these conditions, a quantitative flow cytometry (QFC) assay was performed in parallel with the phantom experiments. This served to validate receptor expression profiles in stimulated and unstimulated tumor cells.

4.3 Results

Three different tissue-mimicking phantom experiments were performed: a cell-free control, one containing untreated lymphoma cells, and a third with lymphoma cells stimulated with IFN- γ . BP analysis yielded an unexpectedly high value in the control condition (2.342) in the cell-free control condition. This was followed by the IFN- γ -treated condition (0.1898), and the lowest binding potential was observed in the untreated condition (0.1753). The fitted binding potential models are graphically represented in Figure 9.

Alongside the tissue-mimicking experiments, QFC was performed to assess the expression levels of PD1, PDL1, and CD80. The results showed that treatment with IFN- γ increased the expression of the three receptors compared to the control condition. Specifically, PD1 expression increased from 22,909 to 27,959 receptors per cell, PDL1 from 2,460 to 3,166 receptors, and CD80 from 2,096 to 4,242 receptors. A comparative illustration of the binding potential between the IFN- γ -treated and untreated conditions is presented in Figure 8.

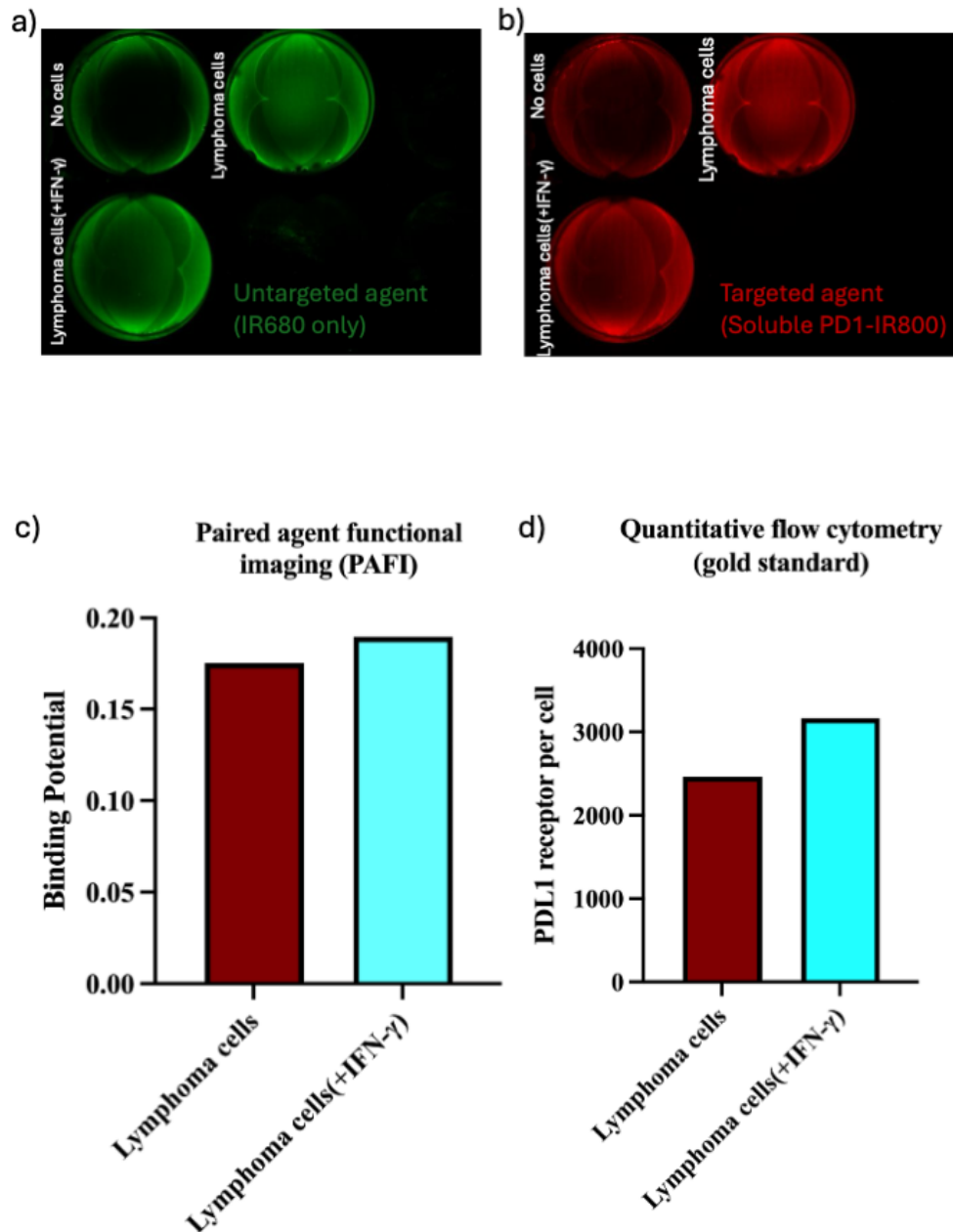


Figure 8. PAFI quantifies functional PDL1 in lymphoma models. (a) Representative images of untargeted and (b) targeted agent signals in tissue-mimicking phantoms with no cells, lymphoma cells, and IFN- γ -treated lymphoma cells after imaging. (c) Bar graphs comparing BP to (d) total PDL1 expression measured by QFC.

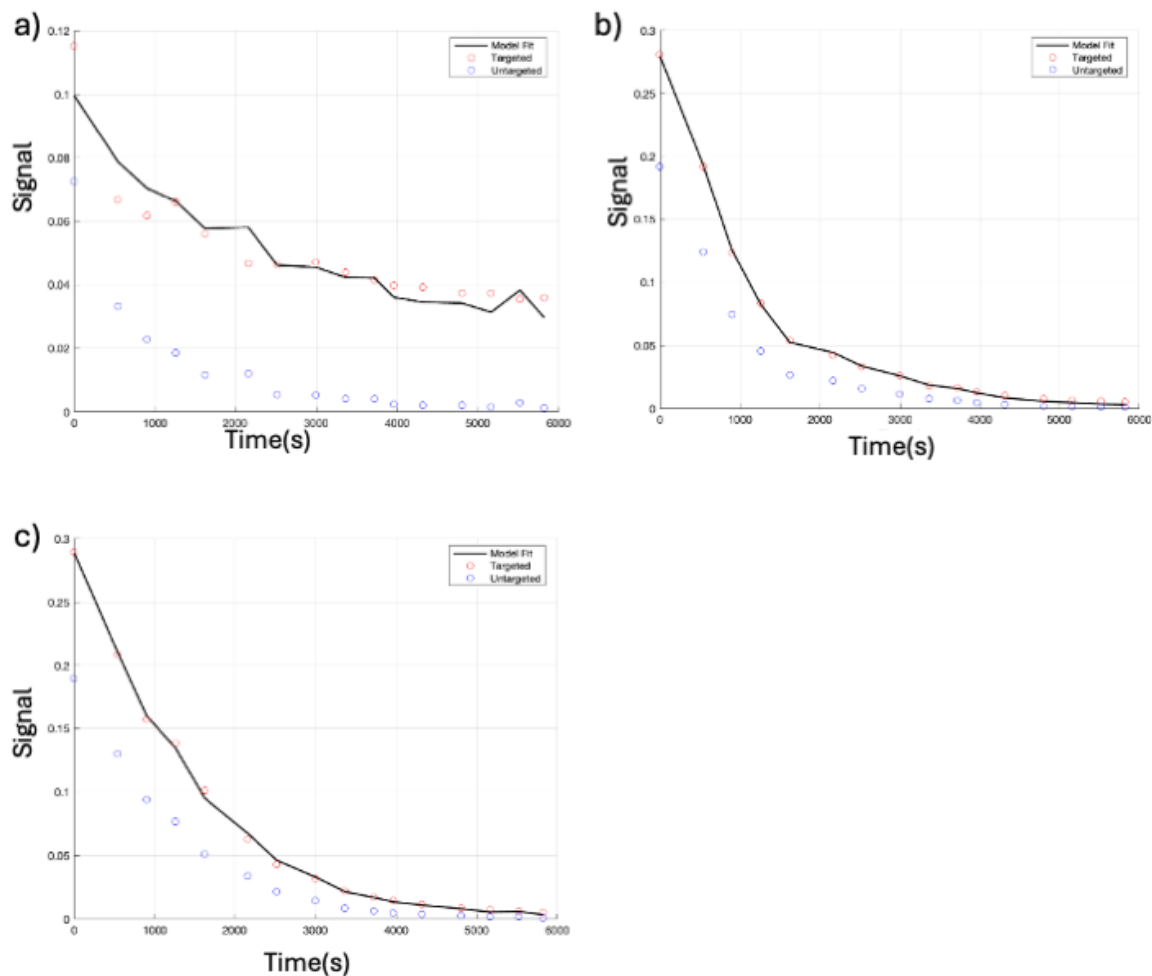


Figure 9. Combination fluorophore experiments set up. (a) Control condition (no cells), (b) IFN- γ -treated lymphoma cells, and (c) untreated Lymphoma cells. In each panel, red circles represent the signal from the targeted agent (PD1-IR800), blue circles indicate the untargeted agent (IR680), and the black line represents the model fit used to calculate binding potential (BP). The calculated BP values were 2.342 for the control, 0.1898 for the IFN- γ -treated condition, and 0.1753 for the untreated condition.

4.4 Discussion

QFC analysis demonstrated that PDL1 expression increased in lymphoma cells following IFN- γ treatment. This observation is consistent with previous studies indicating that IFN- γ upregulates PDL1 expression through activation of the JAK/STAT signaling pathway [13, 14]. Notably, CD80 expression was also upregulated under IFN- γ stimulation. However, only a subset of PDL1 molecules likely formed *cis*-dimers with CD80, leaving a portion of PDL1 available for trans-binding with PD1. This interpretation is supported by findings from Zhao et al. (2019),

who reported that a 3.5-fold molar excess of CD80 is required to block approximately 80% of PDL1:PD1 interactions via cis-binding [15]. These results suggest that while CD80 may partially sequester PDL1, a functionally accessible PDL1 pool likely remains under physiological conditions.

Unexpectedly, the highest binding potential was observed in the control condition (2.342), which lacked cells and was therefore expected to exhibit minimal or no specific binding. This result likely reflects nonspecific accumulation of the targeted or untargeted imaging agents, potentially due to incomplete removal of the dye during PBS rinsing. The IFN- γ -treated condition exhibited a higher binding potential than the untreated condition, suggesting an increased availability of PDL1 in IFN- γ -treated cells. This finding is further corroborated by the corresponding QFC data. These findings emphasize the importance of distinguishing between receptor expression and availability when evaluating immune checkpoint interactions using molecular imaging approaches.

Chapter 5: Future work and global conclusions

5.1 Conclusions

This thesis demonstrates the successful development and application of two distinct PAI methodologies to address critical limitations in assessing immune checkpoint dynamics. First, we established the feasibility of an mPAI framework for the quantitative assessment of total receptor expression for PD1, PDL1, and CD80. Second, we developed a PAI approach utilizing soluble PD1 to specifically quantify the fraction of PDL1 receptors that are functionally available for PD1 binding, a key determinant for the efficacy of immune checkpoint inhibitor (ICI) therapies.

Our findings reveal that IFN- γ treatment up-regulates total PDL1 expression, as confirmed by QFC. The PAI experiments distinctly showed a higher binding potential in IFN- γ -treated conditions compared to untreated cells, directly reflecting an increased available PDL1 pool. By rigorously distinguishing between total receptor expression and functionally accessible receptor populations, this research provides a more dynamic framework for evaluating immune checkpoint interactions.

5.2 Future work for mPAI

The successful development and validation of the tissue mimicking phantom model, along with the determination of the diffusion coefficients, have demonstrated the feasibility of the mPAI approach *in vitro*. Based on these findings, future work should focus on translating this imaging methodology to *in vivo* models. Specifically, implementing mPAI in murine tumor models will

allow the physiological validation of receptor expression patterns and agent behavior in living tissue. Such *in vivo* studies will be instrumental in evaluating the diagnostic potential of mPAI under conditions that reflect the complex tissue architecture and actual tumors. Furthermore, longitudinal imaging could offer insight into dynamic changes in receptor availability over time, further enhancing the utility of mPAI to evaluate immune checkpoint therapy responses.

5.3 Future work for PAI with soluble PD1

In the combination liquid phantom experiments, we observed that the signal intensity of AF700 decreased when combined with AF750 or IR800, despite theoretical expectations that the combined signal would remain constant or increase. This unexpected reduction suggests possible dye–dye interactions, quenching effects, or optical interference. Future studies should explore the physicochemical or spectral interactions between AF700 and other fluorophores.

Furthermore, in tissue-mimicking phantoms, the control condition, which lacked cells, showed an unexpectedly high binding potential of 2.342. In the absence of cellular receptors, the soluble PD1 agent was not expected to bind specifically, and the binding potential should theoretically be zero. This discrepancy suggests possible nonspecific retention of the imaging agents or incomplete removal of unbound dye during the washing steps. Future experiments should implement more rigorous washing protocols and include replicate trials under the same conditions.

To further validate the generalizability of our findings, future studies could also explore PDL1 dynamics across different tumor cell lines, verifying whether the observed binding potential trends are consistently replicated.

Bibliography

- [1] Dong, H., Strome, S. E., Salomao, D. R., Tamura, H., Hirano, F., Flies, D. B., Roche, P. C., Lu, J., Zhu, G., Tamada, K., et al. “Tumor-associated B7-H1 promotes T-cell apoptosis: a potential mechanism of immune evasion”. In: *Nature Medicine* 8.8 (2002), pp. 793–800. doi: [10.1038/nm730](https://doi.org/10.1038/nm730).
- [2] Freeman, G. J., Long, A. J., Iwai, Y., et al. “Engagement of the PD-1 immunoinhibitory receptor by a novel B7 family member leads to negative regulation of lymphocyte activation”. In: *The Journal of Experimental Medicine* 192 (2000), pp. 1027–1034. doi: [10.1084/jem.192.7.1027](https://doi.org/10.1084/jem.192.7.1027).
- [3] Liu, Y., Xia, L., Lin, Y., Wang, Y., Zhang, T., Li, Y., Zhang, Y., Wang, J., Chen, Y., and Xu, J. “PD-L1 *cis*-interaction: A new signaling mechanism in immunoregulation and immunotherapy”. In: *Molecular Cancer* 23.1 (2024), p. 86. doi: [10.1186/s12943-024-02023-w](https://doi.org/10.1186/s12943-024-02023-w). URL: <https://molecular-cancer.biomedcentral.com/articles/10.1186/s12943-024-02023-w>.
- [4] Topalian, S. L., Drake, C. G., and Pardoll, D. M. “Immune Checkpoint Blockade: A Common Denominator Approach to Cancer Therapy”. In: *Cancer Cell* 27.4 (2015), pp. 450–461. doi: [10.1016/j.ccell.2015.03.001](https://doi.org/10.1016/j.ccell.2015.03.001).
- [5] Bruni, D., Angell, H. K., and Galon, J. “The Immune Contexture and Immunoscore in Cancer Prognosis and Therapeutic Efficacy”. In: *Nature Reviews Cancer* 20.11 (2020), pp. 662–680. doi: [10.1038/s41568-020-0285-7](https://doi.org/10.1038/s41568-020-0285-7).
- [6] Haslam, A., Gill, J., and Prasad, V. “Estimation of the Percentage of US Patients With Cancer Who Are Eligible for Immune Checkpoint Inhibitor Drugs”. In: *JAMA Network Open* 3 (2020), e200423. doi: [10.1001/jamanetworkopen.2020.0423](https://doi.org/10.1001/jamanetworkopen.2020.0423).
- [7] Galon, J. and Bruni, D. “Approaches to Treat Immune Hot, Altered and Cold Tumours with Combination Immunotherapies”. In: *Nature Reviews Drug Discovery* 18 (2019), pp. 197–218. doi: [10.1038/s41573-018-0007-y](https://doi.org/10.1038/s41573-018-0007-y).
- [8] Ribas, A. and Hu-Lieskovan, S. “What Does PD-L1 Positive or Negative Mean?” In: *The Journal of Experimental Medicine* 213.13 (2016), pp. 2835–2840. doi: [10.1084/jem.20161462](https://doi.org/10.1084/jem.20161462).
- [9] Chaudhri, A., Xiao, Y., Fitzpatrick, J., Fourestié, A., Sen, M., Bougoüin, A., and al., et. “PD-L1 Binds to B7-1 Only In Cis on the Same Cell Surface”. In: *Immunity* 49.4 (2018), 758–771.e5. doi: [10.1016/j.immuni.2018.09.014](https://doi.org/10.1016/j.immuni.2018.09.014).

- [10] Sugiura, D., Maruhashi, T., Okazaki, I. M., Shimizu, K., Maeda, T. K., Takemoto, T., and Okazaki, T. “Restriction of PD-1 Function by Cis-PD-L1/CD80 Interactions Is Required for Optimal T Cell Responses”. In: *Science* 364.6440 (2019), pp. 558–566. doi: [10.1126/science.aav7062](https://doi.org/10.1126/science.aav7062).
- [11] Tichauer, K. M., Wang, Y., Pogue, B. W., and Liu, J. T. C. “Quantitative in vivo cell-surface receptor imaging in oncology: kinetic modeling and paired-agent principles from nuclear medicine and optical imaging”. In: *Physics in Medicine and Biology* 60.14 (2015), R239–R269. doi: [10.1088/0031-9155/60/14/R239](https://doi.org/10.1088/0031-9155/60/14/R239). URL: <https://doi.org/10.1088/0031-9155/60/14/R239>.
- [12] Xu, X., Wang, Y., Xiang, J., Liu, J. T. C., and Tichauer, K. M. “Rinsing paired-agent model (RPAM) to quantify cell-surface receptor concentrations in topical staining applications of thick tissues”. In: *Physics in Medicine and Biology* 62.12 (2017), pp. 5098–5113. doi: [10.1088/1361-6560/aa6cf1](https://doi.org/10.1088/1361-6560/aa6cf1). URL: <https://doi.org/10.1088/1361-6560/aa6cf1>.
- [13] Garcia-Diaz, A., Shin, D. S., Moreno, B. H., Saco, J., Escuin-Ordinas, H., Rodriguez, G. A., Zaretsky, J. M., Sun, L., Hugo, W., Wang, X., Parisi, G., Saus, C. P., Torrejon, D. Y., Graeber, T. G., Comin-Anduix, B., Hu-Lieskovan, S., Damoiseaux, R., Lo, R. S., and Ribas, A. “Interferon Receptor Signaling Pathways Regulating PD-L1 and PD-L2 Expression”. In: *Cell Reports* 19.6 (2017), pp. 1189–1201. doi: [10.1016/j.celrep.2017.04.031](https://doi.org/10.1016/j.celrep.2017.04.031). URL: <https://doi.org/10.1016/j.celrep.2017.04.031>.
- [14] Mitsuiki, N., Schwab, C., and Grimbacher, B. “What did we learn from CTLA-4 insufficiency on the human immune system?” In: *Immunological Reviews* 287.1 (2019), pp. 33–49. doi: [10.1111/imr.12721](https://doi.org/10.1111/imr.12721).
- [15] Zhao, Y., Lee, C. K., Lin, C., Gassen, R. B., Xu, X., Huang, Z., Xiao, C., Bonorino, C., Lu, L., Bui, J. D., and Hui, E. “PD-L1:CD80 Cis-Heterodimer Triggers the Co-stimulatory Receptor CD28 While Repressing the Inhibitory PD-1 and CTLA-4 Pathways”. In: *Immunity* 51.6 (2019), 1059–1073.e9. doi: [10.1016/j.immuni.2019.11.003](https://doi.org/10.1016/j.immuni.2019.11.003).